

The abundances and properties of Dual AGN and their host galaxies in the EAGLE simulations

Yetli M Rosas-Guevara,^{1,2,3*} Richard G. Bower,⁴ Stuart McAlpine,⁴ Silvia Bonoli,^{2,3} Patricia B. Tissera¹

¹*Departamento de Ciencias Físicas, Universidad Andres Bello, Av. República 220, Santiago, Chile.*

²*Centro de Estudios de Física del Cosmos de Aragón, Plaza San Juan 1, Planta 2, E-44001 Teruel, Spain*

³*Donostia International Physics Center (DIPC), Manuel Lardizabal pasealekua 4, 20018 Donostia, Basque Country, Spain*

⁴*ICC, Physics Department, University of Durham, South Road, Durham DH1 3LE, UK*

Accepted XXX. Received YYY; in original form ZZZ

ABSTRACT

We look into the abundance of Dual AGN in the largest hydrodynamical simulation from the EAGLE project. We define a Dual AGN as two active black holes (BHs) with a separation below 30 kpc. We find that only 1 per cent of AGN with $L_{\text{HX}} \geq 10^{42} \text{ erg s}^{-1}$ are part of a Dual AGN system at $z = 0.8 - 1$. During the evolution of a typical binary BH system, the rapid variability of the hard X-ray luminosity on Myr time-scales severely limits the detectability of Dual AGN. To quantify this effect, we calculate a probability of detection, t_{on}/t_{30} , where t_{30} is the time in which the two black holes are separated at distances below 30 kpc and t_{on} , the time that both AGN are visible (e.g. when both AGN have $L_{\text{HX}} \geq 10^{42} \text{ erg s}^{-1}$) in this period. We find that the average fraction of visible Dual systems is 3 per cent. The visible Dual AGN distribution as a function of BH separation presents a pronounced peak at ~ 20 kpc that can be understood as a result of the rapid orbital decay of the host galaxies after their first encounter. We also find that 75 per cent of the host galaxies have recently undergone or are undergoing a merger with stellar mass ratio ≥ 0.1 . Finally, we find that the fraction of visible Dual AGN increases with redshift as found in observations.

Key words: galaxies:active – methods: numerical – quasars: supermassive black holes

1 INTRODUCTION

Supermassive Black Holes (BHs) appear to reside in the centre of all massive galaxies (e.g. [Kormendi & Ho. 2013](#)). If galaxy mergers are expected to be common in a hierarchical Universe ([White & Rees 1978](#)), then BH mergers should be common too. From numerical studies and models, we know now that during galaxies mergers, supermassive BHs follow the trajectory of the nucleus of the host galaxies (see the review of [Colpi et al. 2014](#) and all therein references). Subsequently, a supermassive BH binary (at scales of a few parsecs) is thought to be form. The time that will take the BHs to eventually merge will strongly depend on their environment that will be set by the properties of the host galaxies (e.g. [Mayer et al. 2007](#); [Mayer 2013](#); [Capelo et al. 2015](#)) such as the presence of molecular clouds or stellar clusters (e.g. [Perets & Alexander 2008](#)), the effects of the galaxy axisymmetry and triaxiality (e.g. [Khan et al. 2013](#); [Vasiliev et al. 2014, 2015](#); [Gualandris et al. 2017](#)). While it is observation-

ally difficult to study BH binaries, hints on their evolution can be found in the observational properties of BH pairs, defined to be BHs in interactive galaxies that have not reached the binary stage. Observationally only active BHs can be easily observed, thus many studies have explored the properties of Dual AGN, defined as two active BHs at kpc-scales.

Observational studies suggest that the fraction of Dual AGN is small ([Fu et al. 2011a](#); [Rosario et al. 2011](#)). [Liu et al. \(2011\)](#) found that the fraction of Dual AGN is 1.3 percent within a 30 kpc scale using a large study of optical AGN pairs at $z < 0.16$ with SDSS spectroscopy. However, detecting Dual AGN at kpc scales in the local Universe is not an easy task since observations at high resolution are needed ([Komossa et al. 2003](#); [Hudson et al. 2006](#); [Bianchi 2008](#); [Koss et al. 2011a, 2012](#); [Mazzarella et al. 2012](#); [Shields 2012](#)). For example, using SDSS spectroscopy could affect the detection of Dual AGN at close scales because of the fibre collision limits. Optical surveys also tend to be incomplete ([Hickox et al. 2009](#); [Koss et al. 2011a](#)). To overcome this difficulty, [Koss et al. \(2012\)](#) select moderate luminous AGN in ultra hard-X-rays along with optical observations.

* E-mail: yetli.rosas@dipc.org

They find a much larger Dual AGN fraction: 7.5 percent of their sample are in Dual AGN at a separation of 30 kpcs. The Dual AGN fraction goes down to 1.9 percent when both AGN in the Dual system were only detected using X-ray spectroscopy. Another way to find candidates of Dual AGN is by searching for a double-peaked in the narrow AGN emission lines (e.g. Comerford et al. 2009b, 2011; Barrows et al. 2013). Using this technique along with follow-up observations, Comerford et al. (2015) and Müller-Sánchez et al. (2015) found seven Dual AGN where it was possible to resolve two distinct active nuclei at separations of less than 10 kpcs.

Whether galaxy mergers enhance AGN activity or not is still under debate. Some of the observational studies mentioned above found that Dual AGN tend to be in galaxies suffering mergers. This suggests that galaxy mergers enhance AGN activity, at least, for the most luminous AGN (e.g. Treister et al. 2012; Donley et al. 2018). For instance, Koss et al. (2012) found that the X-ray luminosity of the AGN in Dual systems increases with decreasing galaxy separation, being a galaxy merger the key to activate the AGN. Similarly, Comerford et al. (2015) found that Dual AGN in major mergers are more luminous than AGN hosted by no interacting galaxies. On the contrary, other works (e.g. Cisternas et al. 2011; Schawinski et al. 2012; Hernández-Ibarra et al. 2016; Villforth et al. 2017) find that galaxy mergers do not have a significant role in the AGN activity.

From the numerical point of view, hydrodynamics simulations of idealised galaxy mergers at high resolution have been used to investigate the Dual AGN activity at the different evolutionary stages of a galaxy merger (e.g. Blecha et al. 2013; Van Wassenhove et al. 2014; Capelo et al. 2017). For example, Capelo et al. (2017), based on the work by Van Wassenhove et al. (2012), study the importance of the merger conditions and the properties of the host galaxies on the Dual AGN. By varying the initial mass ratio, the gas fraction and the geometries of the merger, they find the Dual AGN activity increases after the late pericentric passage. Blecha et al. (2017) also use hydrodynamics simulations along with dust radiative transfer to explore the mid-IR AGN signatures during the late evolutionary stages of a galaxy merger. Although these studies are very insightful to understand Dual AGN activity in galaxy mergers, they miss the effect of the environment and then the occurrence of the Dual AGN in a cosmological context.

The new generation of cosmological hydrodynamics simulations are currently the best tools available to study the incidence of Dual AGN and what drives their activity in a cosmological context. Previous numerical studies have found Dual AGN to be rare as well. For instance, Steinborn et al. (2016) use a large simulation with a volume of $(182 \text{ Mpc})^3$ from the suite of Magneticum Pathfinder Simulations, to compare very close Dual AGN systems to non-active BH pairs and to offset AGN. They define as a BH pair with only one BH active as offset AGN. Steinborn et al. (2016) found a Dual AGN fraction to be less than 1 per cent of the total number of AGN at $z = 2$. The non-active BH pairs in their simulation accrete less gas from the intergalactic medium than Dual AGN. Volonteri et al. (2016), using the horizon-AGN simulation found that the fraction of Dual AGN living in the same host galaxy with a < 30 kpc separation is 0.1 per cent at $z = 0$ for relative massive

galaxies independently on whether these galaxies host an AGN or not. This fraction increases to 2 per cent at $z = 1$. They explore the occupation fraction of BHs as a function of stellar mass, finding that the fraction of Dual systems rises as distances become small. In the context of Dual AGN evolution, Tremmel et al. (2017) follow the evolution of a single Dual AGN (with distances below 1 kpc) in the most massive halo in the Romulus simulation with a volume of only $(8 \text{ Mpc})^3$. They find that this Dual AGN is activated by a major merger.

An interesting question that arises is the cause of the low frequency of Dual AGN. It is because Dual AGN is an ephemeral phase due to the AGN intrinsic properties such as its variability or it is because of the particular properties of the host galaxies of Dual AGN, such as their stellar mass or their gas fraction or it is because of the particular merger history of the host galaxies. To shed further light on this, our main goal is to investigate the pure theoretical predictions in the abundance of Dual AGN in X-ray bands for the hydrodynamical cosmological simulation EAGLE. A series of papers have analysed the galaxy population in EAGLE finding reasonable agreement with the evolution of the galaxy mass functions (Furlong et al. 2015), the evolution of galaxy sizes (Furlong et al. 2017), the colour-magnitude diagram (Trayford et al. 2016), the properties of molecular and atomic gas (Lagos et al. 2015; Bahé et al. 2016) and the oxygen abundance gradients of the star-forming disc galaxies (Tissera et al. 2018). The simulation also reasonably reproduces the evolution of the AGN luminosity functions in X-ray bands up to $z = 1$ (Rosas-Guevara et al. 2016) and the different observational trends seen on the plane of star formation and black hole accretion rates (McAlpine et al. 2017).

In this paper, we explore the abundances and properties of Dual AGN in the largest cosmological hydrodynamical simulation of the EAGLE project (Schaye et al. 2015; Crain et al. 2015) at $z = 0.8 - 1$. We also explore the properties of the host galaxies and their recent merger history. The outline is as follows. In section 2, we describe the simulations and the post-processing analysis to identify Dual AGN. In section 3.1, we show the evolution of a Dual AGN as a study case. In section 3.2, we explore the effects of AGN variability in the detection of a Dual AGN. The Dual AGN fraction as a function of separation is shown in section 3.3. We also investigate the properties of their host galaxies and their recent merger histories in section 3.4, and in section 3.5 we look into the abundances of Dual AGN as a function of redshift. Finally, in section 4 and 5, we discuss and summarise our findings.

2 METHODOLOGY

2.1 Simulations

The Evolution and Assembly of GaLaxies and their Environment (EAGLE, Schaye et al. 2015; Crain et al. 2015)¹ is a suite of cosmological hydrodynamical simulations, comprising various galaxy formation sub-grid models, numerical resolutions and volumes. The simulations were performed with

¹ <http://www.eaglesim.org>

a heavily modified version of SPH code P-Gadget3 (Springel 2005b) that includes: gas cooling, metal enrichment and energy input from star formation and black hole growth. A full description of the simulation suite can be found in Schaye et al. (2015), with the calibration process described in Crain et al. (2015). Here, we concentrate on the largest simulation with a comoving volume² of $(100 \text{ cMpc})^3$, denoted as Ref-L100N1504. The mass resolution is $9.7 \times 10^6 M_\odot$ for dark matter particles and $1.81 \times 10^6 M_\odot$ for baryonic particles and a softening length of 2.66 ckpc limited to a maximum physical size of 0.70 pkpc. The simulation adopts the cosmological parameters taken from Planck collaboration et al. (2013).³

The simulation outputs were analysed using the SUBFIND algorithm to identify bound sub-structures (Springel et al. 2001; Dolag et al. 2009) within each dark matter halo. We identify these substructures as galaxies and measure their stellar and gas masses within a radius of 30 pkpc (as per Schaye et al. 2015).⁴

2.2 Black hole sub-grid physics

Black holes (BH) are seeded into the minimum potential of dark matter halos with masses larger than $1.48 \times 10^{10} M_\odot$. BHs grow via two processes: gas accretion and mergers. The accretion onto BHs is implemented as a modified Bondi prescription, limited to the Eddington rate (Schaye et al. 2015). This modification modulates the high circulation flows with a viscous parameter, C_{visc} , introduced by Rosas-Guevara et al. (2015). A fraction of the accreted mass is converted into thermal energy and released stochastically into the neighbouring gas (Booth & Schaye 2009). The stochastically selected gas particles around the BH are heated by a fixed temperature increment, ΔT , ($= 10^{8.5} \text{ K}$ for the Ref-L100N1504 simulation). We highlight that only a single mode of AGN feedback is adopted, independent of the BH mass or halo mass, using a constant efficiency of 0.1, from which, a fraction of 0.15 is coupled to the interstellar medium.

2.3 Black hole merger criterion

A full description of the black hole merger criterion can be found in Booth & Schaye (2009); Schaye et al. (2015). Given its importance towards this study, here we provide a brief review. A BH merger will occur in EAGLE when the BHs: (1) are separated by a distance below the smoothing kernel and also below three times the gravitational softening length and (2) when the BH relative velocity is lower than the circular velocity at a separation of h_{BH} , $v_{\text{rel}} < (GM_{\text{BH}}/h_{\text{BH}})^{1/2}$, where h_{BH} and M_{BH} correspond to the smoothing kernel

and the subgrid mass of the most massive BH of the system. This criterion avoids a premature BH merger when their host galaxies are starting to merge.

Because the simulation can not adequately model the dynamical friction for BHs with masses below the initial mass of the gas, it is imposed that BHs with $M_{\text{BH}} < 100 m_{\text{gas}}$ are re-located to the minimum of the gravitational potential of the halo. It is also imposed in each step that the BHs change to the position of the neighbouring particle with the lowest gravitational potential of all the neighbouring particles with two conditions: (1) their velocity relative to the BH is smaller than $0.25c_s$ where c_s is the sound speed of the local medium surrounding the BHs, and (2) their distance is smaller than three gravitational softening lengths.

2.4 Dual AGN sample

We make use of the 29 snapshots of the simulations that store the full information of the particles between $z = 20$ and $z = 0$. Following Rosas-Guevara et al. (2016), we take advantage of the ‘snipshots’, that are more frequent outputs of the simulation than the snapshots. The snipshots store a reduced set of the particles properties, but with a finer temporal resolution, ranging between 10 and 60 Myr. We use 200 of these snipshots in this study. We also use the log files that contain properties of the BHs and of their surrounding gas with a much better temporal resolution to capture meticulously the evolution of AGN.

We use the Eddington ratio as a measure of the activity level of BHs defined the Eddington ratio as $\lambda_{\text{Edd}} = \dot{M}_{\text{BH}}/\dot{M}_{\text{Edd}}$, where \dot{M}_{BH} and \dot{M}_{Edd} are the instantaneous BH mass accretion rate and Eddington limit respectively. The BHs with $\lambda_{\text{Edd}} \geq 10^{-2}$ are considered to be prominent sources of luminous X-rays, assuming they are surrounded by a thin and efficient nuclear disc and define them as ‘active’. BHs with λ_{Edd} below this ratio and higher than 10^{-4} are assumed to be enclosed by a thick and inefficient accretion disc and they would not provide a significant contribution of X-ray luminosity. Finally we define an inactive BH when $\lambda_{\text{Edd}} \leq 10^{-4}$. We note that the threshold value taken to define an ‘active’ BH does not significantly affect the evolution of the AGN luminosity functions (see Rosas-Guevara et al. 2016, appendix B).

To remain consistent with the results of Rosas-Guevara et al. (2016) and McAlpine et al. (2017), we define the bolometric luminosity as 10% of the instantaneous mass accretion rate. The bolometric luminosity is converted into hard X-ray luminosity (2-10 keV) using the redshift independent bolometric corrections from Marconi et al. (2004).

We refer to **Dual AGN** as ‘active’ BH pairs with a separation of 30 pkpc or lower. We exclude AGN with lower distances than 1 pkpc since the simulation does not accurately resolve their evolution at such small scales. We create a sample of **visible Dual AGN** where both members of the close pair are accreting at $L_{\text{HX}} \geq 10^{42} \text{ erg s}^{-1}$ in a given snipshot. A **One AGN** sample is also defined where only one member is above this threshold. With this criterium, at $z = 0.8 - 1$, there are 109 Dual AGN, 29 of them belong to the visible Dual AGN sample and 73 to the One AGN sample. The rest of Dual AGN are too faint with a hard X-ray luminosity, L_{HX} , between $10^{40} \text{ erg s}^{-1}$ and $10^{42} \text{ erg s}^{-1}$, and therefore are not visible in this band even though they could

² We will refer to comoving distances with a preceding ‘c’, such as ckpc, to refer to comoving kiloparsec and physical lengths will be preceded by a ‘p’ such as pkpc.

³ The values of the cosmological parameters are: $\Omega_\Lambda = 0.693$, $\Omega_m = 0.307$, $\Omega_b = 0.04825$, $\sigma_8 = 0.8288$, $h = 0.6777$, $n_s = 0.9611$ and $Y = 0.248$.

⁴ The outputs of the simulation are public available by querying the EAGLE SQL web interface <http://icc.dur.ac.uk/Eagle/database.php> (McAlpine et al. 2016)

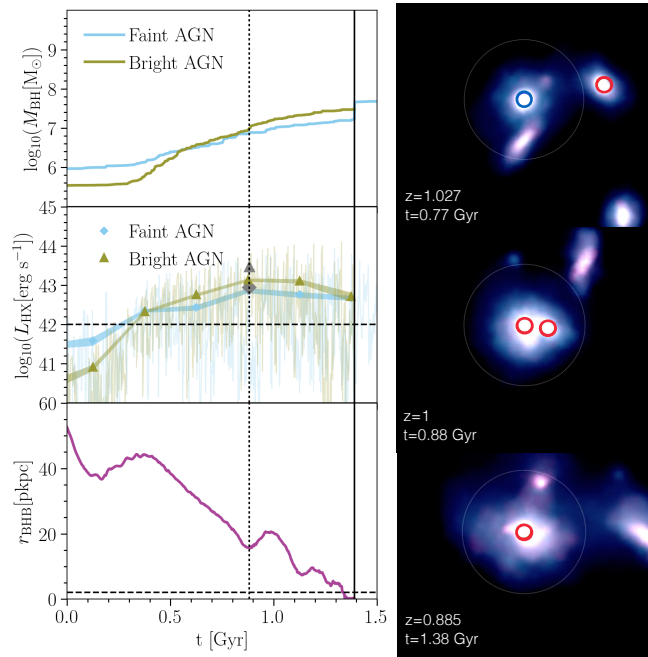


Figure 1. The evolution of a Dual AGN in the EAGLE simulation. *Left figure:* The evolution of the BH mass (top plot), of hard-X-ray luminosity (middle plot) and the BH separation (bottom plot) in the last 1.4 Gyr before the BHs merged. The markers represent the mean luminosity over a 250-Myr-period and the filled region the standard error of the mean. The vertical dashed line represents the time at $z = 1$ and the solid line the time they merged. The grey markers represent the L_{HX} at the moment the Dual AGN was observed ($z = 1$). The horizontal dashed line in the bottom panel is the distance at which the merger criterion is applied. *Right figure:* Images of the host galaxies when the BHs are at separations of ≤ 30 pkpc at different times as indicated on the labels. The circles correspond to the positions of the BHs. For each BH, red circles represent $L_{\text{HX}} \geq 10^{42} \text{erg s}^{-1}$ whereas blue circles the converse. A movie of the evolution of the host galaxies can be found in footnote 5. The evolution shows that the Dual AGN could be variable at scales of Myrs.

be irradiating near the Eddington limit. To give a sense of the BH masses powering visible Dual AGN, the median BH mass is $4.4 \times 10^6 M_{\odot}$ and 70 percent of the BHs have a mass larger than $10^6 M_{\odot}$. The median $M_{\text{BH},1}/M_{\text{BH},2}$, where $M_{\text{BH},1}$ and $M_{\text{BH},2}$ are the masses of less and more massive BH respectively, is 0.1 and 22 percent of the Dual systems have a $M_{\text{BH},1}/M_{\text{BH},2}$ ratio higher than 0.3. We do not make any distinction of Dual AGN with respect to any property of their host galaxy, except in section 3.4.

3 RESULTS

3.1 A study case: The evolution of a Dual AGN system in EAGLE

We begin by illustrating the evolution of a typical Dual AGN observed at $z = 1$. In the left panel of Fig. 1, we show, from top to bottom, the BH mass, hard X-ray luminosity, and AGN separation as a function of cosmic time relative to the merger, where $t = 0$ corresponds to $z = 1.3$. The green and

light-blue curves represent the evolution of the brighter and the fainter AGN, respectively, where the brighter AGN is defined to be so $z = 1$. In the right panel we show a visualisation of the system at three different times (as labelled). These frames are part of a movie⁵ of the host galaxies of the Dual AGN.

At large separations, the BHs have masses within an order of magnitude of the seed mass ($1.48 \times 10^5 M_{\odot}$). Both BHs then gradually acquire mass via gas accretion and they sporadically vary between the states that we defined as ‘Dual AGN’, ‘One AGN’ and an ‘inactive pair’. Note that the average L_{HX} for both BHs is above $10^{42} \text{erg s}^{-1}$ (see the horizontal dashed line) just after 400 Myrs. At this stage, they have comparable BH masses of $6.3 \times 10^6 M_{\odot}$ and $10^7 M_{\odot}$ at $z = 1$ (see the vertical dashed line) in their Dual AGN phase. This is also where the BHs are located in the pericentre of their orbit (see bottom panel).

The BH pair continues to grow by gas accretion funnelled by the galaxy encounter and eventually merge to form a final BH with a mass of $2.7 \times 10^7 M_{\odot}$. Interestingly, the luminosities in the hard X-ray band vary by two orders of magnitude over a temporal scale of megayears as seen in the middle plot. However, overall, the luminosity increases as the BHs get bigger and as their host galaxies get closer to each other (see markers in the middle plot). In the images, the circles represent the location of each AGN, coloured blue if the AGN is too faint to be visible in the hard X-ray band and red when it is visible. The figure shows that the luminosity of both AGN increases on average as the distance between the host galaxies reduces, but also that the presence of rapid AGN variability will significantly reduces the detectability of Dual AGN.

3.2 The Effects of AGN variability

As Fig. 1 has shown, the variability in the AGN luminosity can affect the detection of Dual AGN. To quantify the significance of this effect, we measure t_{on}/t_{30} , where t_{30} is the time the BH pair spend with a separation ≤ 30 pkpc and t_{on} is the time that the BH pair is ‘turned on’ during this period (i.e., when both AGN are accreting at $L_{\text{HX}} \geq 10^{42} \text{erg s}^{-1}$). This ratio, t_{on}/t_{30} , is a proxy for the probability of detecting a Dual AGN: If this ratio is 1, the BH pair is always ‘turned on’. When this ratio is 0 implies that it is impossible to detect the BH pair at these distances.

Fig. 2 shows the cumulative Dual AGN fraction as a function of t_{on}/t_{30} at $z = 0.8 - 1$. The figure illustrates that 60 percent of Dual AGN have a probability of being detected smaller than 0.01 and only 10 percent of Dual AGN are ‘turned on’ for more than 10 percent of the time. With this result, we can estimate the average number of visible Dual AGN respect to the total number of Dual AGN. We found that this average fraction is similar to 3 percent, meaning that from 100 Dual AGN in a given volume, only 3 of them are going to have a hard X-ray luminosity above $10^{42} \text{erg s}^{-1}$.

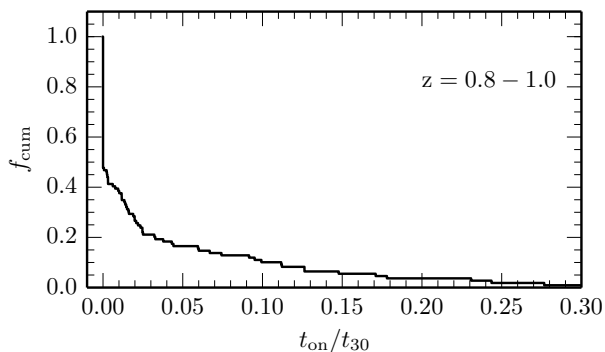


Figure 2. The cumulative Dual AGN fraction as a function of t_{on}/t_{30} at $z = 0.8 - 1$, where t_{on}/t_{30} is the fraction of the time that both AGN in a Dual system are ‘turned on’ during the time they are separated by less than 30 pkpc. This quantity act as a proxy for the detection probability of a Dual AGN. The maximum detection probability that a Dual AGN present is 0.4 and 40 percent of Dual AGN have a detection probability larger than 0.01.

3.3 Incidence of Dual AGN as a function of separation

One of the observational features of Dual AGN that is frequently invoked is their increasing incidence as a function of separation. We investigate this feature by using the visible Dual AGN sample defined in section 2.4.

The top panel of Fig. 3 shows the predicted average fraction of visible Dual AGN as a function of the separation between BHs at $z = 0.8 - 1.0$ (blue solid line). We do not consider Dual AGN with separations smaller than 5 pkpc since their behaviour could be affected by the BH merger criterion (see 2.3)⁶. At small distances (< 15 pkpc), there is no clear trend in the distribution while the Dual AGN fraction presents a pronounced peak located around 20 and 25 pkpc. The presence of the peak is independent of the binsize and the redshift (not shown here). The peak also remains when taking projected distances as shown in the top panel of Fig. 3 (blue dotted line).

To understand its origin, we follow the separation of the BHs and of their host galaxies through time. The bottom panel of Fig. 3 shows that the BHs (green curve) and their host galaxies (blue circles) follow similar trajectories before the galaxy merger takes place. The last close encounter, occurs at 20–25 pkpc and then the host galaxies rapidly spiral inwards, merging at 5–10 pkpc. This last encounter between galaxies could drive gas towards the central parts of the galaxies and feeds the BHs creating a Dual AGN (see section 4). It takes much longer for the BHs to eventually merge, spending more time at closer separations.

The shape of the distribution is also contrasted with the distribution of non active BH pairs (grey line), defining

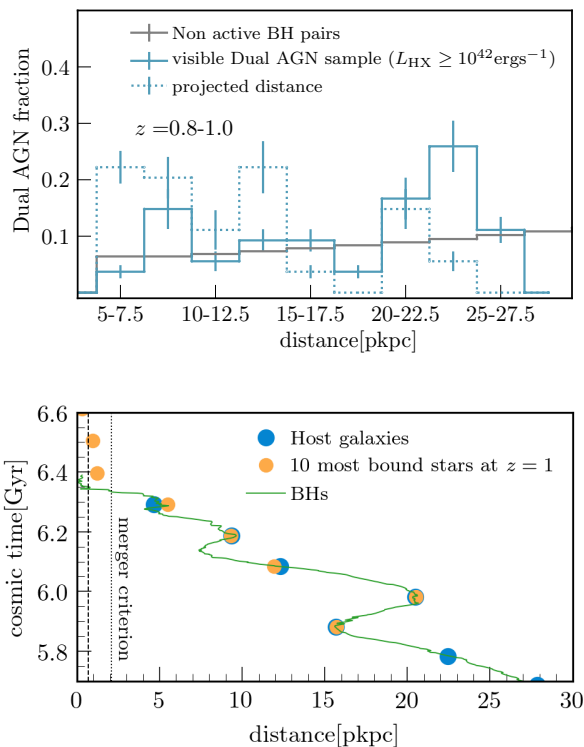


Figure 3. *Top panel:* The normalised distribution of visible Dual AGN as a function of the separation (blue solid line) and projected separation (blue dotted line) at $z = 0.8 - 1$. Bars correspond to the standard errors of the mean using the outputs of the simulation in this redshift bin. We excluded bins below 5 pkpc to avoid sensitivity to the merge criterion in EAGLE. The distribution presents a peak at $\sim 20 - 25$ pkpc. By contrast, the fraction of inactive BH pairs (grey line) increases with increasing separation. *Bottom panel:* A typical example of the cosmic time as a function of separation of the BHs (green line), the centre of the potential of the host galaxies (blue circles) and the ten most bound star particles (orange circles) of each galaxy at $z = 1$. The plot highlights the rapid evolution of the host galaxies of a typical Dual AGN after their last encounter and the small effect of the reposition of the BH.

them as any two BHs whose Eddington ratio is $\leq 10^{-4}$. The fraction of non active BH pairs gradually rises with larger distances contrasting the behaviour of the visible Dual AGN fraction.

Something to note is that the Dual AGN fraction may be affected by the reposition of the BHs to the minimum of the potential of the host halo (see 2.3). To investigate the possible effect of the BH reposition, we follow the trajectories of the 10 most bound star particles of each host halo at $z = 1$ and compare to the trajectories of the BHs. Since the star particles do not undergo any relocation, if the effect of BH repositioning were small, the trajectories of the BHs and of the 10 most bound star particles would be similar. Indeed, we find that in most cases the trajectory of the BHs and of the 10 most bound star particles are almost identical for distances above 5 pkpc. A typical example of this is shown in the bottom panel of Fig. 3. Therefore the BH relocation does not significantly affect the Dual AGN fraction.

⁵ <https://www.cefc.es/owncloud/index.php/s/LXh4I0ikwFimR9H>

⁶ Because the maximum proper softening length is 0.7 pkpc, the merger will take place when the BHs have a distance below 2.1 pkpc

Table 1. The fraction of visible Dual AGN that each resides in a single host galaxy, or two distinct host galaxies, and the fraction of these galaxy subsets that have undergone (or are undergoing) a merger with $f_{M_*} \geq 0.1$ in 2 Gyrs. As an example, if we have 100 visible Dual AGN, in average, 70 of them will be in distinct galaxies from which 57 are undergoing a significant merger.

	total fraction	undergoing /underwent merger with $f_{M_*} \geq 0.1$ in 2 Gyr
Dual AGN in 1 gal	0.30	0.60
Dual AGN in 2 gal	0.70	0.81

Moreover, the BH relocation technique seems to satisfactorily reproduce the BH orbits at kpc-scales.

3.4 Properties of the host galaxies of Dual AGN

In this section, we explore the main properties and the recent merger history of the galaxies that host visible Dual AGN at $z = 0.8 - 1.0$. Firstly, we look at whether the host galaxy/galaxies underwent in the last 2 Gyrs or are undergoing a merger with stellar mass ratio, f_{M_*} , larger than 0.1. Table 1 summarises the recent merger histories of the host galaxies: 30 percent of the visible Dual AGN reside in the same galaxy whereas the remainder in distinct host galaxies that are currently interacting. From the subsample of visible Dual AGN living in the same host galaxy (30 percent of the total sample), 60 percent of their host galaxies experienced a merger with $f_{M_*} \geq 0.1$ in the last 2 Gyr. For the subsample of Dual AGN in distinct galaxies (70 percent of the total sample) the fraction is 0.81. In total, 75 percent of the Dual AGN host galaxies had a major merger in their recent history.

We have also investigated the distribution of stellar masses of the host galaxies of visible Dual AGN and compare to the stellar mass distribution of the galaxies hosting at least one AGN with $L_{\text{HX}} > 10^{42} \text{ erg s}^{-1}$. Visible Dual AGN (blue solid line of Fig. 4, top panel) tend to live in more massive galaxies in comparison with the host galaxies of the full AGN population (grey solid line). The median stellar mass is $\sim 10^{10.5} M_{\odot}$ (blue dotted line) 0.2 dex higher than that of the total AGN population (grey dotted line). Finally, we investigate the gas to stellar mass fractions in the bottom panel of Fig. 4. We compare the median gas to stellar mass fractions (purple solid line with circles) to the one of the host galaxies of visible Dual AGN (green triangles). We find that the galaxies hosting a Dual AGN present higher gas to stellar mass fractions than the median of the distribution, apart from a few cases. These few cases (light green open triangles) are satellites that could have run out of gas because of the interaction with the central galaxy.

3.5 The evolution of the Dual AGN fraction with redshift

Fig. 5 shows that the average fraction of visible Dual AGN (purple solid line). Here, we refer the fraction of visible Dual AGN as the number of AGN that belongs to the visible Dual AGN sample over the total population of AGN with

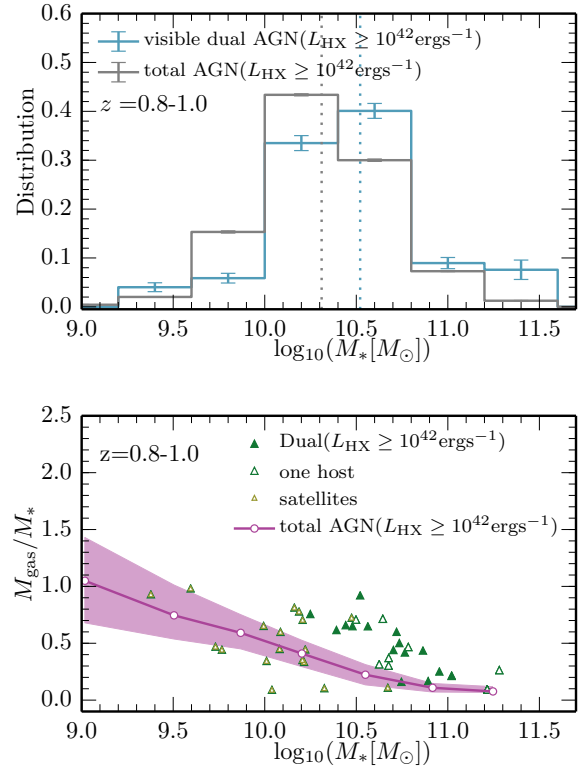


Figure 4. *Top panel:* The stellar mass distribution of the AGN host galaxies at $z = 0.8 - 1.0$. The blue solid line represents the average fraction of galaxies hosting a visible Dual AGN, the grey solid line the galaxies hosting one visible AGN. Bars correspond to the standard error of the media for all the outputs of the simulation in this redshift bin. The error of the mean of the total AGN population is small and not visible. The vertical dotted lines correspond to the median of each population. The plot highlights that visible Dual AGN are relative common in massive galaxies. *Bottom panel:* The gas to stellar mass ratio as a function of stellar mass at $z = 0.8 - 1.0$. The purple solid line with circles represents the median gas to stellar mass ratio in the host galaxies with a visible AGN. The coloured region represents the 30th and 70th percentiles of the distribution. The dark green open triangles correspond to the individual galaxies hosting a visible Dual AGN, the dark green filled triangles to the central galaxy of the Dual systems living in interacting galaxies and the light-green open triangles to those that are satellites. Most of the Dual AGN systems live in a galaxy with an unusually high gas to stellar mass ratio, apart from poor gas satellites that are interacting with their central galaxy.

$L_{\text{HX}} > 10^{42} \text{ erg s}^{-1}$. This definition is similar as observational estimates calculate. This fraction increases with redshift, from 0.1 percent at $z = 0.0 - 0.5$ to 3 percent at $z = 4 - 5$. If one of the AGN of the Dual system is only visible in the hard X-ray band (i.e. the One AGN sample), the average fraction of Dual AGN increases for a given redshift as the green line shows. For instance at $z = 0.8 - 1.0$, it increases from 1 to 2 percent. Note, however, that the average always remains small at all redshifts ($\lesssim 5\%$).

We perform a qualitative comparison of our results with the current observations in the local Universe. Koss et al. (2012) (empty stars) combine X-ray and optical observations to detect close Dual AGN (distance $\leq 30 \text{ pkpc}$), finding a

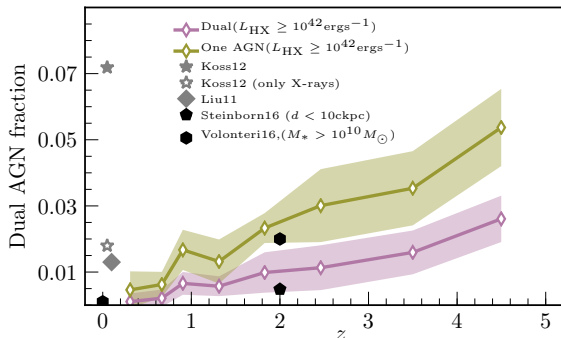


Figure 5. The fraction of visible Dual AGN (purple solid line) and One AGN (green line) as a function of redshift. The coloured regions correspond to the standard deviation. Observational estimates are presented as grey stars (Koss et al. 2012, not filled) and grey diamonds (Liu et al. 2011). Numerical estimates as black pentagons (Steinborn et al. 2016) and hexagons (Volonteri et al. 2016). The plot illustrates an increasing trend in the Dual AGN fraction with redshift and it is much lower compared to observations of the local Universe.

Dual AGN fraction of 7.5 percent. The Dual AGN sample of Koss et al. (2012) detected with X-ray spectroscopy and not with emission lines diagnostics, decreases to 2 percent (filled stars). Liu et al. 2011 (diamonds) use a sample from the Seventh Data Release of the SDSS survey at $z = 0.1$ based on diagnostic emission line ratios. They estimate a Dual AGN fraction with separations ≤ 30 pkpc, to be 1.3 percent. These fractions are marginally above the simulation prediction. This could be due to the different selections and methods used to find Dual AGN in these studies whose estimates are also discrepant to each other by similar margins. Nonetheless, in both observations and the simulation, Dual AGN are rare.

We additionally include estimates from other cosmological hydrodynamical simulations. Steinborn et al. (2016) estimate the fraction of very close Dual AGN (separations of ≤ 10 ckpc) at $z = 2$ from a simulation that is part of the Magneticum Pathfinder set. This simulation has a similar resolution to that from EAGLE with a larger volume, but only run to $z = 2$. They consider an AGN to be a BH powering at $L_{\text{bol}} \geq 10^{43} \text{ erg s}^{-1}$ ($L_{\text{HX}} \gtrsim 10^{42} \text{ erg s}^{-1}$). They found a Dual AGN fraction of 0.5% (pentagon), that is below our prediction but it is consistent because they only consider very close Dual AGN (< 0.33 pkpc). Volonteri et al. (2016) also estimate a Dual AGN fraction (hexagons) $z = 0$ and $z = 2$, in the cosmological hydrodynamic simulation Horizon-AGN. The volume and resolution of the simulation are similar to EAGLE, but they calculate the Dual AGN fraction differently. They calculate the number of AGN with $L_{\text{bol}} \geq 10^{43} \text{ erg s}^{-1}$ and hosted by a single galaxy with stellar mass $\geq 10^{10} M_{\odot}$ over the whole population of galaxies above this stellar mass threshold, independently if they host an AGN or not. The discrepancy between the predictions of EAGLE and Horizon-AGN could be due to the different definition of the Dual AGN fraction. Beside this, they also find an increasing trend with redshift.

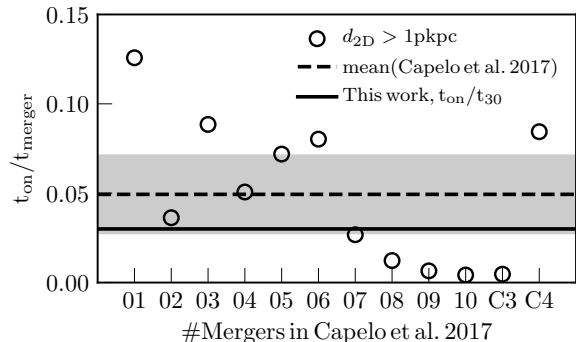


Figure 6. The dual-activity time of the 12 simulations of idealised galaxy mergers from Capelo et al. 2017 normalized by the merger time (initially at a separation 90 pkpc) at projected distances larger than 1 pkpc and with bolometric luminosity larger than $10^{43} \text{ erg s}^{-1}$. The dashed line corresponds to the median and the shaded region to the 2-sigma error of the median. The solid line corresponds to the probability of detect a Dual AGN in this work. This is similar to the dual-activity time of our Dual AGN but normalised for the time the BHs spend in a separation of 30 pkpc or lower. We find that our estimate is roughly consistent with this work.

4 DISCUSSION

In this section, we compare our results to high-resolution hydrodynamical simulations of idealised galaxy mergers (e.g. Van Wassenhove et al. 2012; Capelo et al. 2017; Blecha et al. 2017). We discuss the possible effects of the subgrid physics on the results. Finally, we briefly discuss the main mechanisms that could transport gas in the central part of the galaxies during the merger.

4.1 Comparison to other works using simulations of idealised galaxy mergers

The goal of idealised galaxy mergers simulations is to study the effects of mergers on the galaxy properties at small scales. These simulations have been also used to study the activity of Dual AGN during a merger. For instance, Blecha et al. (2017) study AGN activity during a major merger by mimicking mid-infrared WISE observations. They determine the possible factors that could affect the detection of a Dual AGN. The results of these studies are complementary to our work since cosmological simulations operate on larger scales.

Recently, Capelo et al. (2017) perform a suite of 12 high-resolution simulations of idealised galaxy mergers, similar to the setup of Van Wassenhove et al. (2012). In their study, the galaxies have initial mass ratios larger than 0.1 and disc gas mass fractions of 30 and 60 per cent with different initial geometries of the galaxy encounter (see their Table 1 for the details of each simulation). They define dual-activity time as the time that both AGN are turned on during the merger, normalised by the duration of the merger. They consider that the merger starts when the BH pair is separated by 90 pkpc. This relates to our probability of detection, however, we normalise by the time when the BH pair is first separated by 30 pkpc (see section 3.2). The difference in the definitions

can cause some discrepancies in our results. Fig. 6 shows the dual activity time at projected distances larger than 1 pkpc (just above our resolution limit) and AGN bolometric luminosities larger than $10^{43} \text{ erg s}^{-1}$ (similar to our cut in L_{HX}). As Fig. 6 shows, our estimate is consistent with the results from Capelo et al. (2017) within 2σ errors (shaded region). The small discrepancy between studies could be because our visible Dual AGN sample includes major and minor mergers while their simulations only include major mergers. Also, it is possible that the predictions of the EAGLE simulation underestimate the Dual AGN activity below its spatial resolution.

In agreement with our results, they find that the dual-activity time increases as the BH separations reduce. During the evolution of the merger, there is an increase in AGN activity after the last pericentric stage, agreeable with the peak in the Dual AGN distribution shown in Fig. 3. They also find that the gas fraction has an impact on the Dual AGN activity. This is consistent with our findings in section 3.4, where the primary host galaxy of Dual AGN tends to have higher gas mass fractions than the median of the total galaxy population hosting an AGN. Overall, we are in agreement with most of their findings.

4.2 The effects of the BH merger criterion and resolution

As has been previously mentioned, the distribution of Dual AGN as a function of the BH separation could be affected at small distances because of the BH merger criterion (see 3.3). We investigate its effects on the results of the paper. We obtain similar findings when we exclude Dual AGN at separations below 2.1 pkpc (below this value, the merger criterion could be applied). The population of Dual AGN living in the same host galaxy are dominated by Dual systems with a separation below 2.1 pkpc. However, our main result is preserved since major mergers are also found in the majority of Dual AGN systems. The average fraction of Dual AGN detected is not highly sensitive to the merger criterion. This is because the median fraction of the time that Dual AGN are turned on has a low dependence on the BH separation. This is also present in high-resolution idealised galaxy merger simulations (Capelo et al. 2017) for Dual AGN at low bolometric luminosities. Finally, the increasing trend found in the cosmic evolution of the Dual AGN fraction is preserved, however, the Dual AGN fractions tend to be marginally smaller.

4.3 Other caveats

Something to discuss is the sensitivity of the prediction of EAGLE simulations due to the subgrid physics, particularly, due to AGN and star formation feedback. Crain et al. (2015), in an extensive study, prove that the subgrid physics affect the properties of the galaxies in EAGLE. In their study, they use simulations with a comoving volume of $(25\text{cMpc})^3$ which is far too small for the given frequency of Dual AGN. Although, Rosas-Guevara et al. (2016) compare the evolution of the AGN luminosity functions in hard X-ray bands for three simulations with different subgrid models of star formation and AGN feedback, finding good agreement between

them. Therefore, we expect that the Dual AGN frequency is not significantly affected by the subgrid physics in a cosmological context. Nonetheless, it is something that needs further investigation with improved resolution and larger volumes.

One of our primary results is that galaxy mergers may be a prominent triggering mechanism for Dual AGN activity (see Table 1). This leads us to briefly summarise the possible physical processes that transport gas to the centre of the galaxies during a merger. Using high-resolution idealised galaxies mergers, Blumenthal & Barnes (2018) explore three pure mechanisms (excluding star formation and AGN feedback) during a galaxy merger. These are (1) clump driven inflow (e.g. Duc et al. 2004); (2) ram pressure sweeping (e.g. Capelo & Dotti 2017) and (3) mode driven inflow (e.g. Barnes & Hernquist 1991). They find that the nature of the resulting inflow depends on the geometry of the encounter. They suggest that the main mechanisms could be the clump driven inflow. In this process, shock fronts form after the first pericentric distance and form gas filaments that become Jeans-unstable, forming massive and dense clumps. However, the formation and evolution of these massive and dense clumps could be affected when star formation and AGN feedback are included (e.g. Hopkins et al. 2013).

To test these scenarios in a cosmological context, it would require a more thorough investigation because of the low resolution and the limited volume in the simulations of the EAGLE project. We will reserve this study on a future project that will involve the next generation of hydrodynamical simulations with improved resolution and more realistic physical implementation.

5 SUMMARY

In this paper, we investigate the abundance and evolution of Dual AGN in the EAGLE simulation. We select Dual AGN as black holes (BH) with Eddington ratios ≥ 0.01 , visible in the hard-X-ray band ($L_{\text{HX}} \geq 10^{42} \text{ erg s}^{-1}$) and with a separation less than 30 ckpc. We also explore the main properties of their host galaxies and their recent merger histories. Our main results are as follows:

- We show a study case of the evolution of a typical Dual AGN in the simulation at $z = 1$ in the last 1.4 Gyr before the BHs merge. We find that AGN activity is, overall, triggered by gas funnelled by mergers of their host galaxies. We also find that rapid variability in hard X-ray luminosities at scales of Myrs is present (Fig. 1).
- We explore the effects of AGN variability on the detection of a Dual AGN at $z = 0.8 - 1.0$. We define a probability of detection, t_{on}/t_{30} , where t_{30} is the time that BHs spend within a separation $\leq 30 \text{ pkpc}$ and t_{on} the time that both AGN are ‘turned on’ during this period (i.e., when both AGN have $L_{\text{HX}} \geq 10^{42} \text{ erg s}^{-1}$). We find that 60 percent of our Dual AGN sample have a probability of detection below 1 percent (Fig. 2).
- We obtain the Dual AGN fraction as a function of their BH separation at $z = 0.8 - 1.0$ (Fig. 3). The distribution presents a peak around 20 pkpc. This could be attributed to the fast evolution of the host galaxies after their last encounter, which occurs around this distance. We find similar results for different redshifts and using projected distances.

This could be ascribed to the gas of the central galaxy being accreted by the infall BH in agreement with observations (Lambas et al. 2003; Alonso et al. 2007).

- We explore the main properties of the host galaxies and their recent merger histories. We find that 75 percent of the host galaxies recently undergone or are undergoing a merger with a mass ratio larger than 0.1. We compare the properties of the host galaxies to the total galaxy population hosting an AGN. We find that Dual AGN tend to live in galaxies with higher stellar mass and higher gas to stellar mass fractions. We also find that some of the host galaxies of Dual AGN have a lower gas to stellar mass fraction, but those are satellite galaxies whose BH could be feeding by gas from the central galaxy (Fig. 4).

- The average visible Dual AGN fraction in hard X-ray ($L_{\text{HX}} > 10^{42} \text{ erg s}^{-1}$) increases with redshift (Fig. 5). This rising trend is also found in other numerical and observational works (Comerford & Greene. 2014; Volonteri et al. 2016). When only one of the AGN has $L_{\text{HX}} \geq 10^{42} \text{ erg s}^{-1}$, the average Dual AGN fraction increases.

This paper uses a state-of-the-art cosmological simulation to study the evolution of galaxies. The EAGLE simulation reproduces the observables of galaxies in the local Universe such as stellar masses, colours, sizes. It also reproduces with good agreement the evolution of AGN luminosity functions up to $z = 1$ and the contrasting observed trends of the plane of star formation rate–black hole accretion rate. In this paper, the EAGLE simulation allows us to study in a more statistical mean the frequency of Dual AGN and the effects of AGN variability in the detection of Dual AGN at $z = 0.8 - 1$. Dual AGN tend to be rare and their detection are affected by AGN variability. The enhancement in the fraction of Dual AGN at small scales is a natural result of the evolution of their host galaxies merging. It also confirms earlier suggestions that Dual AGN might be triggered by significant galaxy mergers. Although the evolution of the Dual AGN is not captured at scales below the BH merger criterion is applied in EAGLE, we show that our findings are preserved. Something that it is not completely clear from our work is the conditions of the major mergers to activate a Dual AGN or if major mergers always activate a Dual AGN. In further work, we plan to extend this study in more detail.

ACKNOWLEDGEMENTS

We thank Joop Schaye, Lisa Steinborn, Sergio Contreras and David Izquierdo-Villalba for the useful comments in the first draft and the anonymous referee for constructive feedback that improved the paper. This work was financially supported by Fondecyt 1150334 Conicyt and from the European Union Horizon 2020 Research and Innovation Programme under the Marie Skłodowska-Curie grant agreement No 734374. RGB acknowledges the Science and Technology Facilities Council (STFC) through grant ST/P000541/1 for support. This work would have not be possible without Lydia Heck's technical support. We acknowledge the Virgo Consortium for making their simulation data available. The EAGLE simulations were performed using the DiRAC-2 facility at Durham, managed by the ICC, and the PRACE

facility Curie based in France at TGCC, CEA, Bruyères-le-Château. This work used the DiRAC Data Centric system at Durham University, operated by the Institute for Computational Cosmology on behalf of the STFC DiRAC HPC Facility (www.dirac.ac.uk). This equipment was funded by BIS National E-infrastructure capital grant ST/K00042X/1, STFC capital grant ST/H008519/1, and STFC DiRAC Operations grant ST/K003267/1 and Durham University. DiRAC is part of the National E-Infrastructure. We thank contributors to SciPy⁷, Matplotlib⁸, and the Python programming language⁹.

REFERENCES

- Alonso, M. S., Lambas, D. G., Tissera, P., & Coldwell, G. 2007, MNRAS, 375, 1017
- Bahé, Y. M., Crain, R. A., Kauffmann, G., et al. 2016, MNRAS, 456, 1115
- Barnes J. E., Hernquist L. E., 1991, ApJ, 370, L65
- Blecha L., Loeb A., Narayan R., 2013, MNRAS, 429, 2594
- Blecha L., Snyder G. F., Satyapal S., Ellison S. L., 2018, MNRAS, 478, 3056
- Blumenthal K. A., Barnes J. E., 2018, MNRAS, 479, 3952
- Bondi H., Hoyle F., 1944, MNRAS, 104, 273.
- Booth C. M., Schaye J., 2009, MNRAS, 398, 53.
- Bianchi S., Chiaberge M., Piconcelli E., Guainazzi M., Matt G., 2008, MNRAS, 386, 105
- Barrows R. S., Sandberg Lacy C. H., Kenneck J., Comerford J. M., Kenneck D., Berrier J. C., 2013, ApJ, 769, 95
- Capelo P. R., Dotti M., Volonteri M., Mayer L., Bellovary J. M., Shen S., 2017, MNRAS, 469, 4437
- Capelo P. R., Dotti M., 2017, MNRAS, 465, 2643
- Comerford J. M., Grith R.L., Gerke B. F et al. 2009b, ApJ, 702, L82
- Comerford J. M., Pooley D., Gerke B. F., Madejski G. M., 2011, ApJ, 737, L19
- Comerford, J. M., & Greene, J. E. 2014, ApJ, 789, 112
- Comerford, J. M., Pooley, D., Barrows, R. S., et al. 2015, ApJ, 806, 219
- Crain, R. A., Schaye, J., Bower, R. G., et al. 2015, arXiv:1501.01311
- Colpi, M. 2014, SSR, 183, 189
- Cisternas M., et al., 2011, ApJ, 726, 57
- Donley J. L., et al., 2018, ApJ, 853, 63
- Dolag K., Borgani S., Murante G., Springel V., 2009, MNRAS, 399, 497
- Duc P.-A., Bournaud F., Masset F., 2004, A&A, 427, 803
- Fu H., Myers A. D., Djorgovski S. G., Yan L., 2011a, ApJ, 733, 103
- Furlong, M., Bower, R. G., Theuns, T., et al. 2015, MNRAS, 450, 4486
- Furlong, M., Bower, R. G., Crain, R. A., et al. 2017, MNRAS, 465, 722
- Gualandris A., Read J. I., Dehnen W., Bortolas E., 2017, MNRAS, 464, 2301
- Hopkins P. F., Narayanan D., Murray N., Quataert E., 2013, MNRAS, 433, 69
- Hernández-Ibarra F. J., et al., 2016, MNRAS, 459, 291
- Hudson D. S., Reiprich T. H., Clarke T. E., Sarazin C. L., 2006, A&A, 453, 433
- Hickox, R. C., et al. 2009, ApJ, 696, 891

⁷ <http://www.scipy.org>

⁸ <http://www.matplotlib.sourceforge.net>

⁹ <http://www.python.org>

Kormendy J., Ho L. C., 2013, *ARA&A*, 51, 511

Khan F. M., Holley-Bockelmann K., Berczik P., Just A., 2013, *ApJ*, 773, 100

Komossa S., Burwitz V., Hasinger G., Predehl P., Kaastra J. S., Ikebe Y., 2003, *ApJ*, 582, L1

Koss, M., et al. 2011a, *ApJL*, 735, L42

Koss, M., Mushotzky, R., Treister, E., et al. 2012, *ApJl*, 746, L22

Lagos, C. d. P., Crain, R. A., Schaye, J., et al., 2015, *MNRAS*, 452, 3815

Lambas, D. G., Tissera, P. B., Alonso, M. S., & Coldwell, G. 2003, *MNRAS*, 346, 1189

Liu, X., Shen, Y., Strauss, M. A., & Hao, L. 2011, *ApJ*, 737, 101

Marconi, A. and Risaliti, G. and Gilli, R. and Hunt, L. K. and Maiolino, R. and Salvati, M., 2004, *MNRAS*, 351, 169.

McAlpine, S., Helly, J. C., Schaller, M., et al. 2016, *Astronomy and Computing*, 15, 72

McAlpine, S., Bower, R. G., Harrison, C. M., et al. 2017, *MNRAS*, 468, 3395

Müller-Sánchez F., Comerford J. M., Nevin R., Barrows R. S., Cooper M. C., Greene J. E., 2015, *ApJ*, 813, 103

Capelo, P. R., Volonteri, M., Dotti, M., et al. 2015, *MNRAS*, 447, 2123

Mayer, L., Kazantzidis, S., Madau, P., et al. 2007, *Science*, 316, 1874

Mayer, L. 2013, *Classical and Quantum Gravity*, 30, 244008

Mazzarella J. M., et al., 2012, *AJ*, 144, 125

Planck Collaboration and Ade, P. A. R. and Aghanim, N. and Alves, M. I. R. and Armitage-Caplan, C. and Arnaud, M. and Ashdown, M. and Atrio-Barandela, F. and Aumont, J. and Aussel, H. and et al., 2013, *arxiv e-prints*, 1303.5062.

Perets, H. B., & Alexander, T. 2008, *ApJ*, 677, 146

Rosario D. J., McGurk R. C., Max C. E., Shields G. A., Smith K. L., Ammons S. M., 2011, *ApJ*, 739, 44

Rosas-Guevara Y. M., Bower R.G., Schaye J., et al. 2015, *MNRAS*, 454, 1038

Rosas-Guevara, Y., Bower, R. G., Schaye, J., et al. 2016, *MNRAS*, 462, 190

Salcido, J., Bower, R. G., Theuns, T., et al. 2016, *MNRAS*, 463, 870

Schaye, J., Crain, R. A., Bower, R. G., et al. 2015, *MNRAS*, 446, 521

Schawinski K., Simmons B. D., Urry C. M., Treister E., Glikman E., 2012, *MNRAS*, 425, L61

Shields G. A., Rosario D. J., Junkkarinen V., Chapman S. C., Bonning E. W., Chiba T., 2012, *ApJ*, 744, 151

Springel V., Di Matteo T. and Hernquist L., 2005a, *MNRAS*, 361, 776.

Springel V., White S. D. M., Tormen G., Kauffmann G., 2001, *MNRAS*, 328, 726

Springel, V., 2005b, *MNRAS*, 364, 1105.

Steinborn, L. K., Dolag, K., Comerford, J. M., et al. 2016, *MNRAS*, 458, 1013

Tissera P. B., et al., 2018, *ArXiv e-prints*, arXiv:1806.04575

Trayford, J. W., Theuns, T., Bower, R. G., et al. 2016, *arXiv:1601.07907*

Tremmel, M., Karcher, M., Governato, F., et al. 2017, *MNRAS*, 470, 1121

Treister E., Schawinski K., Urry C. M., Simmons B. D., 2012, *ApJ*, 758, L39

Van Wassenhove S., Volonteri M., Mayer L., Dotti M., Bellovary J., Callegari S., 2012, *ApJ*, 748, L7

Van Wassenhove S., Capelo P. R., Volonteri M., Dotti M., Bellovary J. M., Mayer L., Governato F., 2014, *MNRAS*, 439, 474

Vasiliev E., Antonini F., Merritt D., 2014, *ApJ*, 785, 163

Vasiliev E., Antonini F., Merritt D., 2015, *ApJ*, 810, 49

Villforth C., et al., 2017, *MNRAS*, 466, 812

Volonteri, M., Dubois, Y., Pichon, C., & Devriendt, J. 2016, *MNRAS*, 460, 2979

White, S. D. M. and Rees, J. M., 1978, *MNRAS*, 183, 341

This paper has been typeset from a \LaTeX file prepared by the author.